



Contents lists available at ScienceDirect

## Organic Electronics

journal homepage: [www.elsevier.com/locate/orgel](http://www.elsevier.com/locate/orgel)

## Trap-limited mobility in space-charge limited current in organic layers

José M. Montero<sup>a</sup>, Juan Bisquert<sup>a,\*</sup>, Germà Garcia-Belmonte<sup>a</sup>, Eva M. Barea<sup>a</sup>, Henk J. Bolink<sup>b</sup><sup>a</sup> Photovoltaic and Optoelectronic Devices Group, Departament de Física, Universitat Jaume I, 12071 Castelló, Spain<sup>b</sup> Institut de Ciència Molecular, Universitat de València, Polígon La Coma s/n, 46980 Paterna, València, Spain

## ARTICLE INFO

## Article history:

Received 28 July 2008

Received in revised form 11 November 2008

Accepted 29 November 2008

Available online 10 December 2008

## Keywords:

OLED

Transport in organic materials

Trap

Mobility

Impedance

Capacitance

## ABSTRACT

Space-charge limited current transport in organic devices, relevant to the operation of a range of organic optoelectronic devices, is analyzed in the frequency domain. The classical multiple trapping picture with one transport state and one trap level is used as the basis for the descriptions. By varying the energetic and kinetic properties of the traps, we show that the admittance and the capacitance spectra are considerably modified depending on the interplay between the trap-limited mobility and the trap kinetics. We point out that capacitance steps at low-frequency, usually found in experiments, are observed only for slow traps.

© 2008 Elsevier B.V. All rights reserved.

## 1. Introduction

The discovery of electroluminescence in organic materials [1] launched a vast research effort for improving the performance and stability of organic semiconductors applied in optoelectronic devices such as organic light-emitting diodes (OLEDs) [2]. Polymer-based OLEDs are quite appealing for their easy processability by spin coating and ink-jet printing techniques [3]. However, further understanding of the physical behavior of such materials is needed. For instance, the description of the charge transport in organic layers by space-charge limited current (SCLC) model requires to include field [4–6] or density-dependent [7] mobility according to the percolation models [8]. Experimentally, the determination of transit times in single-carrier devices has been widely used to measure the mobility by time-of-flight (TOF) [9] and impedance spectroscopy techniques [10,11], among others [12]. It has also been recognized that the role of energetic disorder is crucial for an adequate knowledge and control of the

properties of organic transport layers. Transport in a single-carrier device has been often rationalized in terms of an extended state and a distribution of traps in the band-gap [13–15]. In this approach, the traps produce a decrease of the transport rate in the extended states [16]. However, in general the dynamics of traps is far more complex, since the traps relaxation intersects with the transport features throughout the layer [17]. While the trapping-diffusion dynamics can be solved completely in homogeneous situations [18], the typical carrier distribution at high injection currents in an organic layer in the SCLC regime is highly inhomogeneous [19].

The aim of this paper is to go beyond a quasistatic approximation to the trap-limited mobility (in which free and trapped charge remain in local equilibrium [13,20]) and to treat rather generally an apparently simple problem, a two level system composed of a transport state and a single trap level. The advantage of this model is that we can fully classify the different dynamic regimes of the system by the interplay of the relevant kinetic constants. This gives us physical insight in the interpretation of more general systems with a distribution of localized levels (e.g., exponential or Gaussian) which can be calculated

\* Corresponding author.

E-mail address: [bisquert@fca.uji.es](mailto:bisquert@fca.uji.es) (J. Bisquert).

numerically, a method also applied to dual-carrier devices [10,21,22]. However, the latter systems are beyond the scope of this paper.

The problem treated in this paper has been already considered some decades ago by Dascalu [23,24] and Kassing [25,26], for the particular case of a slow-shallow trap (i.e., when the transit time is shorter than trapping time) and this case is also solved numerically in the present paper. In addition, we consider the dynamic results in the frequency domain for fast traps, and also for deep traps. By formulating a general analytical model valid for a fast-shallow trap, we find a delay in the transit time (and thus, a mobility decrease) due to multiple trapping, as measured by means of impedance techniques [27].

The paper has the following structure. Firstly, a mathematical description is presented of the single-trap model, secondly, physical implications according to the applications of the model are discussed, and finally, we provide the main conclusions.

## 2. Single-trap model

The SCLC for single-carrier transport (neglecting diffusion) of electrons in a transport level with density  $n_c$  that drift in the electric field  $F$ , a trap level of occupancy  $f_t$  and total density  $N_t$ , is described by: the continuity equation, the drift-current equation, Poisson equation and the trap dynamics equation, respectively [9,18]

$$\frac{dJ}{dx} = 0 \quad (1)$$

$$J = q\mu_0 n_c F + \varepsilon_r \varepsilon_0 \frac{\partial F}{\partial t} \quad (2)$$

$$\frac{dF}{dx} = \frac{q}{\varepsilon_r \varepsilon_0} (n_c + N_t f_t) \quad (3)$$

$$\frac{\partial f_t}{\partial t} = cn_c [1 - f_t] - ef_t \quad (4)$$

Here  $q$  is the elementary charge,  $\mu_0$  is the mobility,  $\varepsilon_r \varepsilon_0$  the dielectric constant, and  $c$  and  $e$  are the coefficients for electron capture and release, respectively. The potential can be calculated by integrating the electrical field along the thickness  $L$

$$V = \int_0^L F dx \quad (5)$$

The population of the extended states at the energy level  $E_c$ , for a non-degenerate semiconductor, relates to the Fermi level  $E_F$  as

$$n_c = N_c e^{(E_F - E_c)/k_B T} \quad (6)$$

where  $N_c$  is an effective density of states in the transport level (conduction band). Assuming that the trap level at energy  $E_t$  reaches equilibrium with the extended states (with the same Fermi level), the trap occupancy is given by

$$f_t = \frac{1}{1 + e^{(E_t - E_F)/k_B T}} \quad (7)$$

In steady state, Eq. (4) gives

$$f_t = \frac{1}{1 + e/(cn_c)} \quad (8)$$

Therefore, the detailed balance condition provides the following relationship for the trap emission and capture coefficients:

$$e = cN_c e^{(E_t - E_c)/k_B T} \quad (9)$$

Let us denote steady-state by  $\bar{x}$  and small perturbation by  $\hat{x}$  applied at a certain angular frequency  $\omega$ . Therefore every electrical variable can be expressed as  $x = \bar{x} + \hat{x}$  to linearize the whole system of equations up to the first order [28,29]. As shown in Ref. [17], by solving Eq. (4) for a small perturbation, we obtain

$$\hat{f}_t = \frac{1}{\bar{n}_c} \frac{\bar{f}_t(1 - \bar{f}_t)}{1 + i\omega/\omega_t} \hat{n}_c \quad (10)$$

This term gives the contribution to the spectra of the capacitance and conductance of the trap. The trap frequency is defined as

$$\omega_t = \frac{e}{1 - \bar{f}_t} \quad (11)$$

This is the maximum frequency that the trap is acting as such, since at higher frequencies the trap cannot follow the ac perturbation, as will be described in Section 3. Inserting Eq. (9) in Eq. (11), we find the dependence of  $\omega_t$  on the trap energy and the occupation, as

$$\omega_t = \frac{cN_c e^{(E_t - E_c)/k_B T}}{1 - \bar{f}_t} \quad (12)$$

It should be remarked that in the SCLC regime,  $\bar{f}_t$  is position-dependent along the organic layer. The impedance is defined as the quotient of potential to current density,

$$Z(\omega) = \frac{\hat{V}(\omega)}{\hat{J}(\omega)} \quad (13)$$

$\hat{V}(\omega)$  is determined by spatial integration of  $\hat{F}(\omega)$  from the solution of the above described model. The boundary conditions at the injecting contact used to solve the electrical variables along the thickness in  $dc$  and  $ac$  conditions are [30,31]

$$\bar{n}_c(x=0) = N_c \text{ and } \hat{F}(x=0) = 0 \quad (14)$$

Capacitance and conductance are defined as follows:

$$C'(\omega) = \text{Re} \left[ \frac{1}{i\omega Z(\omega)} \right] \quad (15)$$

$$g(\omega) = \text{Re} \left[ \frac{1}{Z(\omega)} \right] \quad (16)$$

## 3. Results and discussion

In this section we show the results of the calculations of the capacitance and the conductance spectra for different trap properties and voltages, compared to the trap-free case. We first describe the latter case as a reference, and then discuss variations of energetics ( $E_t$ ), by considering a shallow and a deep trap level, and the trap kinetics ( $c$ ),

for a fast and a slow trap. The different configurations are given in Table 1.

### 3.1. Trap-free

The well-known trap free SCLC model with constant mobility is given by the analytical expression for stationary and impedance responses as [32]

$$J = \frac{9}{8} \varepsilon \mu_0 \frac{V^2}{L^3} \quad (17)$$

$$Z(\omega) = \frac{6}{g_0(i\omega\tau_0)^3} \left[ 1 - i\omega\tau_0 + \frac{1}{2}(i\omega\tau_0)^2 - \exp(-i\omega\tau_0) \right] \quad (18)$$

where the transit time, the geometrical capacitance and the conductance are, respectively,

$$\tau_0 = \frac{4}{3} \frac{L^2}{\mu_0 V} \quad (19)$$

$$C_g = \frac{\varepsilon}{L} \quad (20)$$

$$g_0 = \frac{dJ}{dV} = \frac{3}{\tau_0} C_g \quad (21)$$

For low-frequency, the admittance is

$$Y(\omega) = g_0 + i\omega \frac{3}{4} C_g \quad (22)$$

and for high-frequency it is

$$Y(\omega) = \frac{2}{3} g_0 + i\omega C_g \quad (23)$$

It is well-known that the capacitance spectrum makes a step from  $\frac{3}{4}C_g$  to  $C_g$  at around the transit time frequency, i.e., when the small perturbation of charge carriers injected by the frequency perturbation voltage is able to arrive at the collecting contact. However, in experimental data, this ideal behavior is usually distorted, mainly at low-frequencies, by the trap contribution to capacitance.

### 3.2. Steady-state characteristics of organic layers with shallow and deep traps

Experimental measurements of  $J$ - $V$  curves have been used to determine the transport properties in organic layers [33,34]. Simulations of current density–voltage curves and the Fermi level distributions are displayed in Fig. 1 for two different trap energy configurations. These results are well understood and described in the literature [35]. For a shallow trap, the trap population is much less than the population of the transport level, hence the electric field distribution is not significantly altered, causing only a slight variation in the Mott–Gurney square law

$$J \approx \frac{9}{8} \varepsilon \theta \mu_0 \frac{V^2}{L^3} \quad (24)$$

where  $\theta$  is a carrier-density dependent factor of trapped and free charge defined as [27]

$$\theta^{-1} = \left( 1 + \frac{\langle \bar{n}_t \rangle}{\langle \bar{n}_c \rangle} \right) \quad (25)$$

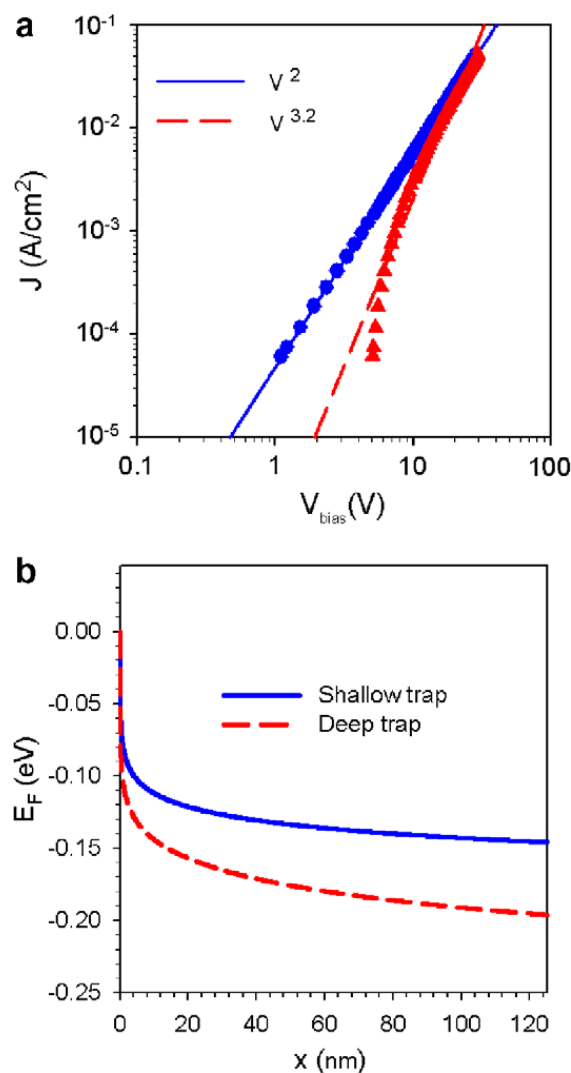


**Fig. 1.** Model simulations of shallow ( $E_c - E_t = 0.1$  eV) and deep ( $E_c - E_t = 0.5$  eV) trap configurations represented by blue solid lines and red dashed lines. (a) Current density voltage-characteristics for a shallow trap and a deep trap are plotted by blue dots and red triangles. Fittings provide the exponent of the voltage. (b) Fermi level representations at 6 V along the thickness, for a shallow trap (blue solid line) and a deep level (red dashed line). (For interpretation of the references to colour in this figure legend, the reader is referred to the web version of this article.)

with the brackets denoting an average over the thickness of the film. For a deep trap, the occupancy of the trap level increases and the trapped charges play a crucial role in the current density–voltage curves. At low bias, most carriers are trapped, thus significantly altering the carrier and electric field distributions with respect to trap-free case, leading to an abrupt increase of the current slope,  $J \propto V^m$  with  $m \geq 2$ . At high bias, the trapping sites are already filled and all the additional injected carriers are located in the transport level. This situation bends the curve from a higher voltage exponent than 2, towards a square law dependence.

### 3.3. Dynamic characterization of shallow traps

Let us now focus our attention on the dynamic properties of the electrical variables (capacitance and

conductance) in the case of the shallow trap. A general outline of the simulation results is displayed in Fig. 2. To accurately determine the *ac* transit times  $\tau_{ac}$ , it is worth to apply the representation of negative differential suscep-

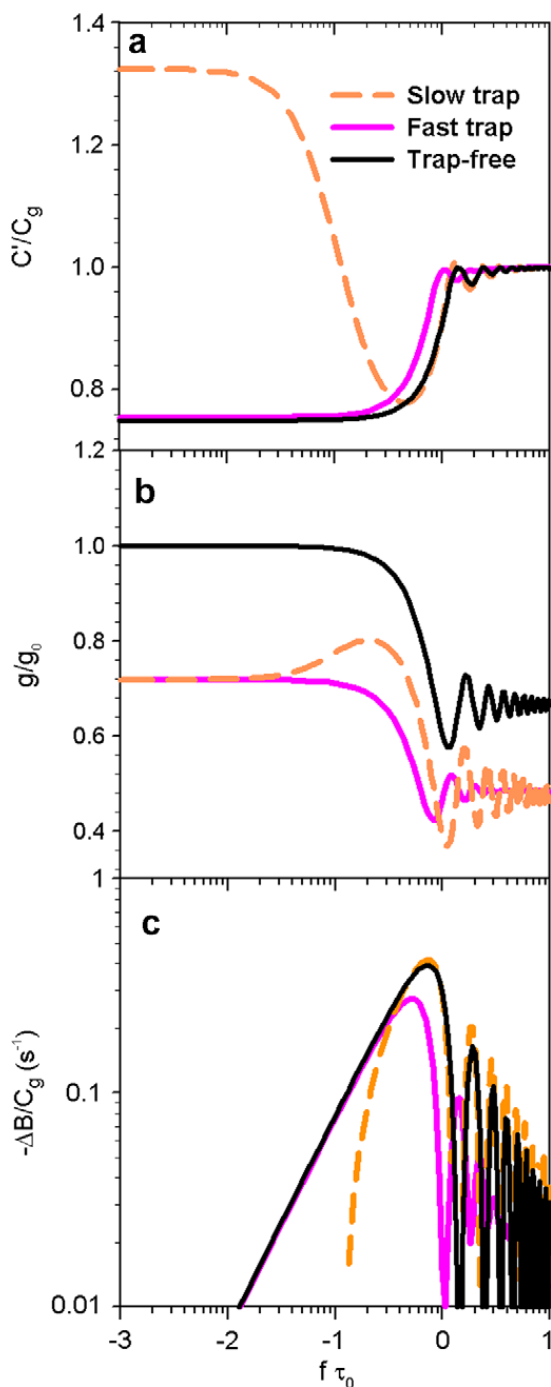


**Fig. 2.** Simulation spectra for shallow traps at 2 V. Fast traps are plotted by pink lines, slow traps by orange dashed lines and trap-free spectrum by black. (a) Capacitance spectra normalized to  $C_g$  for fast and slow traps. Low-frequency increase is displayed for slow traps whereas not for the fast ones. (b) Conductance spectra normalized to  $g_0$  for fast and slow traps. (c) Negative differential susceptance  $-\Delta B(\omega)$  normalized to  $C_g$  to extract transit times. In the case of fast trapping, *ac* transit time is  $\tau_{ac} = 1.36\tau_0$  ( $\tau_0 = 221.6 \mu\text{s}$ ) with  $\theta^{-1} \approx 1.40$ , whereas for slow trapping no deviation from the trap free is observed. (For interpretation of the references to colour in this figure legend, the reader is referred to the web version of this article.)

tance ( $-\Delta B(\omega) = \text{Im}(Y(\omega)) = -\omega(C'(\omega) - C_g)$ ), that provides peaks at certain frequencies  $f_{\max}$  such that [36]

$$\tau_{ac} \approx 0.72 \cdot f_{\max}^{-1} \quad (26)$$

Fig. 2a shows the capacitance spectra (normalized to  $C_g$ ) for the trap-free case, as a reference, and a shallow trap with two different trap kinetics, fast and slow (as specified below). At low-frequencies, the presence of a shallow trap in the organic layer implies (1) a deviation of the capacitance spectra for the slow case, and (2) of transit time for the fast one. At high frequencies, all the spectra converge to  $C_g$  with smooth and decaying oscillations as theoretically expected. In experiments, a slight decrease of the capacitance occurs due to the dielectric relaxation of the material [37].

As for conductance, Fig. 2b, the normalized low-frequency value decreases by a factor  $\theta$  and the calculated *ac* transit time (normalized to  $\tau_0$ ) is increased by  $\theta$ , although only for fast traps, thus in Fig. 2b we obtain for low-frequencies  $g = 0.71g_0$  and for high frequencies,  $g = 2\theta g_0/3$ . All these behaviors will be modeled and explained in terms of a quasi-equilibrium between the two states (trapping and transport levels) in the forthcoming subsections.

#### 3.4. Fast-shallow traps

When the trap kinetics is fast, quasi-equilibrium prevails between carriers in the trap and transport levels. In this case we expect the standard formula of Rose [27] for trap limited transport to be valid

$$\mu = \theta\mu_0 \quad (27)$$

and therefore, the trap-limited transit time is

$$\tau = \theta^{-1}\tau_0 \quad (28)$$

In order to check Eq. (27), in Fig. 3 changes in the population of the traps were imposed by modifying  $N_t$ . The resulting capacitance spectra are well described by the trap-free case formulas by using the trap-limited values  $\tau$  and  $g$  instead of  $\tau_0$  and  $g_0$ . In particular we obtain

$$g = \frac{dJ}{dV} = \frac{3}{\tau} C_g = \theta g_0 \quad (29)$$

The inset of Fig. 3 shows that Eq. (28) is indeed satisfied.

The physical interpretation of this situation is given in terms of the interplay between trapping and detrapping and the carrier transit time. If fast-shallow traps are present in an organic layer, a delay in the transit time is expected and thereby, a mobility decrease. An experimental method to corroborate whether this kind of energetic disorder exists, consists on the evaluation of the *ac* transit time from admittance spectroscopy, Eq. (26), and the *dc* transit time, Eq. (19). The possible deviation should be attributed to the presence of fast-shallow traps.

#### 3.5. Slow-shallow traps

If the trapped charge is not able to achieve the quasi-equilibrium with the carrier concentration in the transport

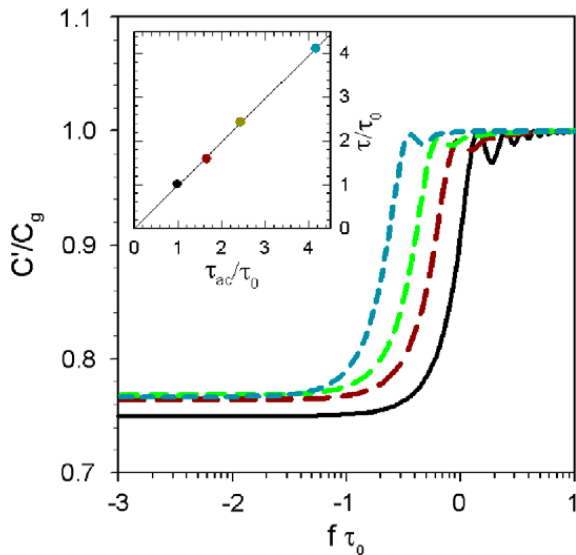


**Fig. 3.** Simulated capacitance spectra steps for fast-shallow traps at 6 V ( $\tau_0 = 73.8 \mu\text{s}$ ) with varying trap densities, from left to right:  $N_t = 8 \times 10^{17}$ ,  $4 \times 10^{17}$ ,  $2 \times 10^{17}$ ,  $0 \text{ cm}^{-3}$ . Inset shows an identification of the transit times between the models discussed in the text, and the  $ac$  conductance calculation.

levels, the spectra present a large low-frequency capacitance that increases above the  $3C_g/4$  value, Fig. 4. When exceeding the trap frequency  $\omega_t$  of Eq. (11), capacitance rapidly decreases as trapping action ceases for the rest of the frequency range. In contrast to the previous case, here carriers are able to cross the organic layer and reach the collecting contact before being trapped, avoiding any delay and following the trap-free transit time  $\tau_0$ . Dascalu and Kassing have given the analytical expression for the impedance in this situation [23–26]

$$Z(\omega) = \frac{6\alpha}{g_0} \sum_{k=0}^{\infty} \frac{\Gamma(\theta\alpha + 1)}{\Gamma(\theta\alpha + k + 2)} \frac{(-i\omega\tau_0)^k}{k + 3} \quad (30)$$

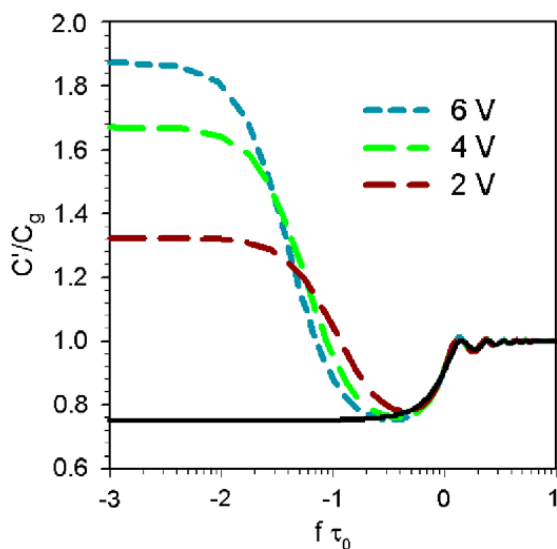


**Fig. 4.** Model representations of the capacitance spectra for slow-shallow traps at voltages 6, 4 and 2 V, from top to bottom. The trap-free spectrum is pictured in black.

with  $\alpha$  being

$$\alpha(\omega) = 1 + \frac{\omega_c}{\omega_e} \frac{1}{1 + i\omega/\omega_e} \quad (31)$$

Here  $\omega_c = c(N_t - \langle \bar{n}_t \rangle)$  and  $\omega_e = \beta(\langle \bar{n}_c \rangle + N_c e^{(E_t - E_c)/k_B T})$  are the reciprocal lifetimes for electrons in the conduction band and in the trap level, respectively. For low-frequency with  $N_t \gg \langle \bar{n}_t \rangle$ , we have the approximation [26]

$$Y(\omega) = g + i\omega \frac{C_g}{\omega_e \tau_0} \quad (32)$$

being  $g = \theta g_0$  and for high-frequency

$$Y(\omega) = \frac{2}{3}g + i\omega C_g \quad (33)$$

The low-frequency capacitance increase is usually found in experiments for single-carrier devices [11,38,10] and, according to our model, due to the slow-shallow trap contribution. The model also predicts a coincidence in transit times by  $ac$  and  $dc$  techniques unlike the previous case.

In Fig. 5, it is shown that the low-frequency capacitance dependence with the voltage exhibits a peak when quasi-Fermi level crosses the trap energy level ( $E_t$ ) corresponding to a maximum in the trap contribution to the capacitance, Eq. (10). The low-frequency conductance is similar to the trap-free value at high voltages since free charges dominate the injected carrier concentration.

### 3.6. Limit between fast- and slow-shallow traps

In the previous subsection, we have shown two extreme behaviors dominated either by transit or trapping time. It is interesting to establish the conditions that determine which regime prevails. Let us define the trap and transit time frequencies as

$$\langle \omega_{tr} \rangle \approx \frac{cN_c e^{(E_t - E_c)/k_B T}}{1 - \langle \bar{f}_t \rangle} \quad (34)$$

$$\omega_{tt} = 2\pi/\tau_0 \quad (35)$$

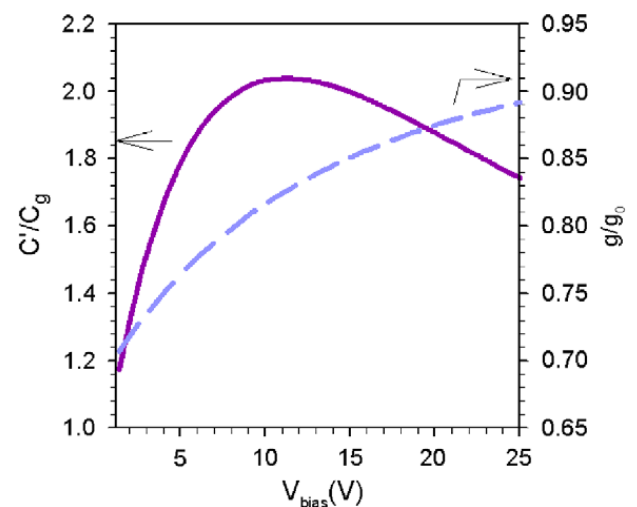


**Fig. 5.** Calculations of the low-frequency capacitance (violet solid line) and conductance (cyan dashed line) versus voltage at 1 Hz. (For interpretation of the references to colour in this figure legend, the reader is referred to the web version of this article.)

If the trap frequency is larger than the reciprocal transit time, the fast trap regime with the multiple trapping transit time  $\tau = \theta^{-1}\tau_0$  is present. In the opposite situation, the slow trap regime occurs with the trap-free transit time  $\tau_0$  value.

Inserting Eqs. (34) and (35) in  $\langle\omega_{tr}\rangle \approx \omega_{tt}$ , it is possible to quantify a critical capture coefficient  $c_c$  as

$$c_c \approx \frac{2\pi}{\tau_0} \frac{1 - \langle\bar{f}_t\rangle}{N_c e^{(E_t - E_c)/k_B T}} \quad (36)$$

According to the parameters of Table 1, this quantity is estimated as  $c_c \approx 10^{-13}$  cm<sup>3</sup>/s. If a trap capture coefficient is lower than this critical value the trap is slow, whereas if it is higher, the trap is fast. In Fig. 6, normalized transit times are plotted versus normalized trap frequency and both transit time regimes are depicted showing a narrow transition from the trap-free formula to the multiple trapping one.

As pointed out at the end of Section 3.4, to experimentally determine if shallow traps of an organic layer are slow or fast, the technique consists in comparing the transit times from *ac* (Eq. (26)) and *dc* (Eq. (19)). A coincidence would give us the slow result whereas a deviation indicates the presence of fast traps.

**Table 1**  
Material parameters used in the simulation of transport in an organic layer.

<i>L</i> (nm)	$N_c$ (cm <sup>-3</sup> )	$\mu_0$ (cm <sup>2</sup> /(Vs))	$E_t$ (eV)	$N_t$ (cm <sup>-3</sup> )	$c$ (cm <sup>3</sup> /s)
125	10 <sup>19</sup>	4.7 × 10 <sup>-7</sup>		10 <sup>17</sup>	
Trap properties	Shallow	-0.1	Fast	10 <sup>-12</sup>	
	Deep	-0.5	Slow	10 <sup>-14</sup>	

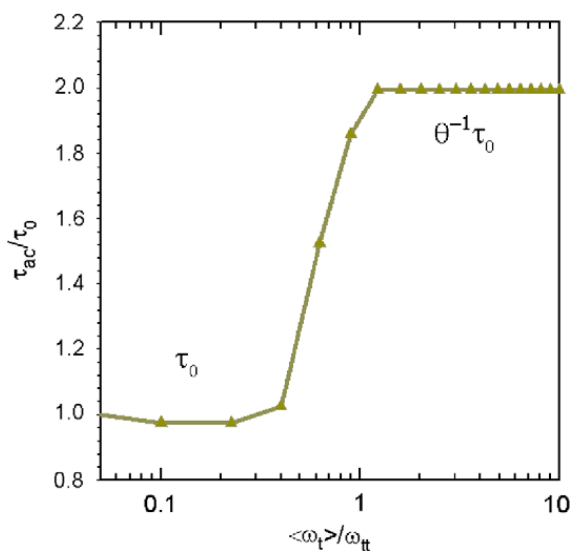


**Fig. 6.** Simulations of normalized transit times calculated from the *ac* conductance method versus normalized trap frequency at 6 V and  $N_t = 3 \times 10^{17}$  cm<sup>-3</sup>, describing a step up from the classical transit time  $\tau_0 = 73.8$   $\mu$ s to the multiple trapping one,  $\tau_{ac} = \theta^{-1}\tau_0$  with  $\theta^{-1} \approx 2$ . Classical transit time occurs for normalized trap frequency ( $\omega_{tt} = 85$  kHz)  $\langle\omega_t\rangle/\omega_{tt} < \theta$  and multiple trapping for  $\langle\omega_t\rangle/\omega_{tt} > 1$  according to dotted vertical marks.

### 3.7. Comparison between dynamic and static capacitance

Dynamic capacitance, obtained from admittance spectroscopy at low-frequencies, is frequently compared to the well-known static one [13]. In SCLC, the low-frequency capacitance has a value of  $3C_g/4$  [32,39], whereas the static capacitance is set at  $3C_g/2$  [13]. This reduced factor of 1/2 in the dynamic capacitance is attributed to the three contributions to the *ac* current (velocity modulation, density modulation and displacement term) [26]. In a two level system with a shallow trap, the static capacitance is calculated by integrating the charge stored in the device per voltage unit as [13]

$$C_{st} = \frac{q}{V} \left( \int_0^L \bar{n}_c(x) dx + \int_0^L \bar{n}_t(x) dx \right) \quad (37)$$

where *V* is the bias applied along the organic layer. In Fig. 7, the static capacitance is plotted versus bias-voltage. It is observed that the value remains at  $3C_g/2$  as in the trap-free case. At low voltages, the capacitance contribution essentially comes from the majority of the charge stored in the shallow trapping sites whereas at high voltages the capacitance is mainly due to free charge.

### 3.8. Dynamic characterization of deep traps

In contrast to the shallow trap energy level, where occupation is quite low, in the case of a deep trap, the opposite situation occurs as occupation is approaching the unity. This deviation strongly determines the contribution to the impedance from the trap dynamics Eq. (4). The trap levels are so heavily occupied that the temporal variation of  $\bar{f}_t$  is governed by the emitting rather than the trapping term. The numerical solution for the capacitance and the conductance is shown in Fig. 8a and b displaying distinct features with respect to the trap-free spectrum: a

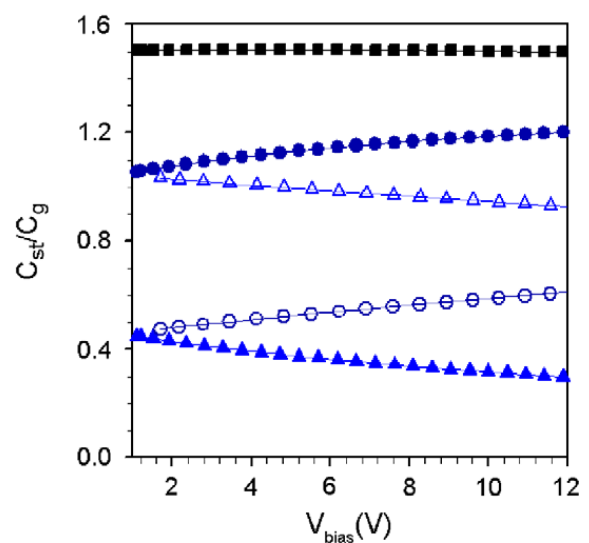


**Fig. 7.** Model calculations of the static capacitance versus voltage for a shallow trap (black squares). Free carrier contribution (solid and empty triangles) and trap carrier contribution (solid and empty circles) to static capacitance. Solid and empty symbols are for  $N_t = 1 \times 10^{17}$ ,  $5 \times 10^{17}$  cm<sup>-3</sup>, respectively.

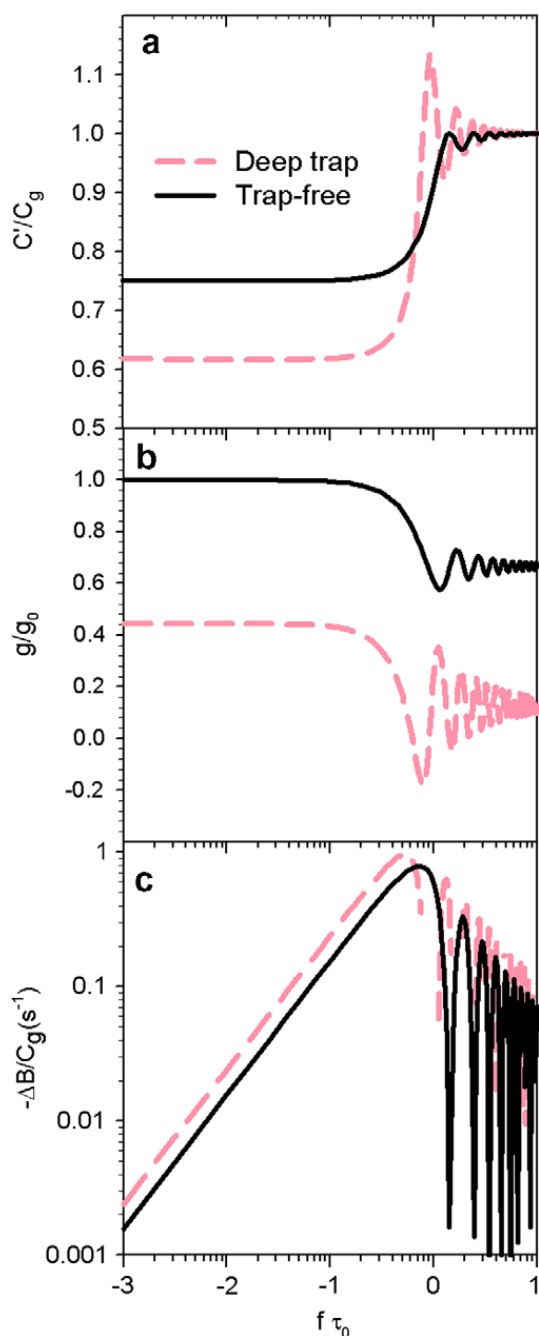


**Fig. 8.** Model solution of impedance spectra for deep trap at 6 V. Traps are plotted by maroon dashed lines and trap-free spectrum in black as a reference. (a) Capacitance spectra normalized to  $C_g$ . (b) Conductance spectra normalized to  $g_0$ . (c) Negative differential susceptance  $-\Delta B(\omega)$  normalized to  $C_g$ .

low-frequency capacitance below  $3C_g/4$ , a conductance spectrum significantly lower, and increased oscillation in the transition from low to high frequencies. These results are independent of the traps kinetics, which is another particularity in comparison to the shallow-trap results.

#### 4. Conclusions

The single-trap model has been described and numerically solved for SCLC for impedance studies in order to

determine the dynamical properties of carrier transport and storage depending on energy (shallow and deep) and kinetics (fast and slow) of the trap. For a fast-shallow trap, an analytical model is provided and validated by means of the multiple trapping formula for mobility  $\mu = \theta\mu_0$ , where  $\theta$  depends on the steady-state solution (trapped and free charge). For a slow-shallow trap, the available analytical model has been revised. Both regimes, fast and slow, have been characterized depending on the dominance of either trapping or transit processes and an experimental method has been also provided by comparing *dc* and *ac* transit times. A deep trap results in a decrease in the low-frequency capacitance (with respect to the trap-free case) and also in a delay in the transit times.

#### Acknowledgements

We thank financial support from MEC of Spain under programs: Consolider-Ingenio 2010 (Project HOPE CSD2007-00007), "Ramón y Cajal", FPI (Project MAT2004-05168) and ESF-EUROCORES project 05-SONS-FP-021 (MAT2006-28187-E). We are also grateful to the support from Bancaixa (Project P1 1B2005-12). We appreciate discussions with Dan Dascalu.

#### References

- [1] J.H. Burroughes, D.D.C. Bradley, A.R. Brown, R.N. Marks, K. MacKay, R.H. Friend, P.L. Burn, A.B. Holmes, *Nature* 347 (1990) 539.
- [2] S. Forrest, *Nature* 428 (2004) 911.
- [3] Y. Shen, A.R. Hosseini, M.W. Wong, G.G. Malliaras, *Chem. Phys. Chem.* 5 (2004) 16.
- [4] H. Bässler, *Phys. Status Solidi (b)* 175 (1993) 15.
- [5] P.N. Murgatroyd, *J. Appl. Phys.* D 3 (1970) 151.
- [6] P.S. Davids, I.H. Campbell, D.L. Smith, *J. Appl. Phys.* 82 (1997) 6319.
- [7] C. Tanase, P.W.M. Blom, D.M. Leeuw, *Phys. Rev. B* 70 (2004) 193202.
- [8] M.C.J.M. Vissenberg, M. Matters, *Phys. Rev. B* 57 (1998) 12964.
- [9] P.W.M. Blom, M.C.J.M. Vissenberg, *Mater. Sci. Eng. R27* (2000) 53.
- [10] D. Poplavskyy, F. So, *J. Appl. Phys.* 99 (2006) 033707.
- [11] H.H.P. Gommans, M. Kemerink, G.G. Andersson, R.M.T. Pijper, *Phys. Rev. B* 69 (2004) 155216.
- [12] S. Shirota, H. Kageyama, *Chem. Rev.* 107 (2007) 953.
- [13] B. Ramachandhran, H.G.A. Huizing, R. Coehoorn, *Phys. Rev. B* 73 (2006) 233306.
- [14] M.M. Mandoc, B. de Boer, P.W.M. Blom, *Phys. Rev. B* 73 (2006) 155205.
- [15] V.I. Arkhipov, E.V. Emelianova, G.J. Adriaenssens, *Phys. Rev. B* 64 (2001) 125125.
- [16] A.L. Alvarez, B. Arredondo, B. Romero, X. Quintana, A. Gutiérrez-Llorente, R. Mallavia, J.M. Otón, *IEEE Trans. Electron. Dev.* 55 (2008) 674.
- [17] J. Bisquert, *Phys. Rev. B* 77 (2008) 235203.
- [18] J. Bisquert, V.S. Vikhrenko, *Electrochim. Acta* 47 (2002) 3977.
- [19] G.T. Wright, *Solid-State Electron.* 2 (1960) 165.
- [20] J. Bisquert, *Phys. Chem. Chem. Phys.* 10 (2008) 3175.
- [21] N.D. Nguyen, M. Schmeits, *Phys. Rev. B* 75 (2007) 075307.
- [22] M. Schmeits, *J. Appl. Phys.* 101 (2007) 084508.
- [23] D. Dascalu, *Int. J. Electron.* 21 (1966) 183.
- [24] D. Dascalu, *Solid-State Electron.* 11 (1968) 491.
- [25] R. Kassing, E. Kähler, *Solid State Commun.* 15 (1974) 673.
- [26] R. Kassing, *Phys. Status Solidi (a)* 28 (1975) 107.
- [27] A. Rose, *Concepts in Photoconductivity and Allied Problems*, John Wiley and Sons, 1963.
- [28] A. van der Ziel, *Solid State Physical Electronics*, Prentice-Hall, Englewood Cliffs, 1976.
- [29] W. Brütting, S. Berleb, *Phys. Rev. Lett.* 89 (2002) 286601.
- [30] P.W.M. Blom, M.J.M. de Jong, M.G. van Munster, *Phys. Rev. B* 55 (1997).
- [31] N.F. Mott, R.W. Gurney, *Electronic Processes in Ionic Crystals*, Oxford University Press, London, 1940.

- [32] J. Shao, G.T. Wright, *Solid-State Electron.* 3 (1961) 291.
- [33] A.J. Campbell, M.S. Weaver, D.G. Lidzey, D.D.C. Bradley, *J. Appl. Phys.* 84 (1998) 6737.
- [34] F. So, B. Krummacher, M.K. Mathai, D. Poplavskyy, S.A. Choulis, *J. Appl. Phys.* 102 (2007) 091101.
- [35] M.A. Lampert, *Current Injection in Solids*, Academic Press, New York, 1970.
- [36] H.C.F. Martens, J.N. Huiberts, P.W.M. Blom, *Appl. Phys. Lett.* 77 (2000) 1852.
- [37] H.C.F. Martens, H.B. Brom, P.W.M. Blom, *Phys. Rev. B* 60 (1999) R8489.
- [38] J.M. Montero, J. Bisquert, G. Garcia-Belmonte, H. Bolink, E.M. Barea, *Phys. Status Solidi (a)* 204 (2007) 2402.
- [39] D. Dascalu, *Solid-State Electron.* 12 (1969) 444.